RSC Advances

PAPER

View Article Online
View Journal | View Issue

Check for updates

Cite this: *RSC Adv.*, 2022, **12**, 19209

Modification of silica nanoparticles by 2,4-dihydroxybenzaldehyde and 5-bromosalicylaldehyde as new nanocomposites for efficient removal and preconcentration of Cu(II) and Cd(II) ions from water, blood, and fish muscles

Hanem M. Gad,[a] S. M. El Rayes [a] and Ehab A. Abdelrahman *[b]

Herein, silica nanoparticles were modified by 2,4-dihydroxybenzaldehyde and 5-bromosalicylaldehyde to produce new nanocomposites which were abbreviated as N_1 and N_2, respectively. The synthesized nanocomposites were used for efficient removal and preconcentration of Cu(II) and Cd(II) ions from water, blood, and fish muscles. FE-SEM, FT-IR, XRD, CHN elemental analysis, and nitrogen gas sorption analyzer were used to characterize the new nanocomposites. The XRD proved that the synthesized oxide is cristobalite with an average crystallite size of 54.80 nm. Due to the formation of the C=N group, the intensity of the XRD peak at $2\theta = 21.9°$ in the N_1 and N_2 nanocomposites decreased significantly. The FT-IR bands, which appeared at 1603 and 1629 cm^{-1} in the N_1 and N_2 nanocomposites, are attributable to the bending vibration of C=N and/or OH, respectively. Also, the FE-SEM analysis shows the morphology of the silica nanoparticles which were identified as spherical and rod-like with slight agglomeration while the N_1 and N_2 nanocomposites have flaky surfaces due to the formation of C=N groups. The maximum Cu(II) ion adsorption capacities of the N_1 and N_2 nanocomposites are 64.81 and 40.93 mg g^{-1}, respectively. The maximum Cd(II) ion adsorption capacities of the N_1 and N_2 nanocomposites are 27.39 and 26.34 mg g^{-1}, respectively. The adsorption of Cu(II) or Cd(II) ions using the synthesized nanocomposites is spontaneous, chemical, exothermic, and well-matched with the Langmuir equilibrium isotherm. The recovery findings demonstrate that the preconcentration process is accurate, adaptable, and resulted in quantitative separation because % Recovery is more than 95%. Furthermore, the % RSD was less than 3.5%, indicating good reproducibility.

Received 19th May 2022
Accepted 24th June 2022

DOI: 10.1039/d2ra03177a

rsc.li/rsc-advances

Open Access Article. Published on 01 July 2022. Downloaded on 2/7/2026 3:15:04 PM.
This article is licensed under a Creative Commons Attribution-NonCommercial 3.0 Unported Licence.

1. Introduction

The release of toxic metals, which are produced from different industries, into the environment causes global concern due to its harmful effect on aquatic organisms, humans, soil, and plants.[1–3] Cadmium and its compounds are highly toxic where exposure to them causes cancer and damages the cardiovascular system, digestion, breathing, reproductive system, kidneys, and nerves.[4–6] Excess amounts of copper may cause liver and brain poisoning, diarrhea, skin rashes, anemia caused by red cell breakage, high blood pressure, heart disease, premenstrual syndrome, nausea, stomach pain, and severe damage to the central nervous system. Excess amounts of copper also accompany psychological and mental illnesses such as autism, behavior problems, hyperactivity in children, depression in adults, dementia, and stuttering.[7–9] Pollution with heavy metals such as copper and cadmium is the most dangerous type of pollution as a result of their accumulation in the organs of fish or plants. Hence, human consumption of large quantities of fish or plants, that contain high concentrations of heavy metals, leads to human poisoning.[10–12] Maximum allowed concentrations of Cd(II) and Cu(II) in water as recommended by the World Health Organization (WHO) are 3 and 2 μg L^{-1}, respectively.[13,14] Until now, heavy metals have been removed and determined using many methods such as precipitation, evaporation, electrochemical, and membrane separation.[15–18] Unfortunately, these methods display several disadvantages involving low efficiency, high cost, and secondary damage to the water environment.[19] Consequently, it is essential to find an economical and environmentally friendly method for removing and preconcentrating heavy metals from water. The adsorption method is familiar as an efficient and simple method for removing and preconcentrating heavy metals from water.[20–26] The adsorption mechanism is typically dependent on the chemical or physical

[a]*Chemistry Department, Faculty of Science, Suez Canal University, Ismailia 41522, Egypt*

[b]*Chemistry Department, Faculty of Science, Benha University, Benha 13518, Egypt. E-mail: dr.ehabsaleh@yahoo.com; ehab.abdelrahman@fsc.bu.edu.eg; Tel: +201010636875*

© 2022 The Author(s). Published by the Royal Society of Chemistry

Open Access Article. Published on 01 July 2022. Downloaded on 2/7/2026 3:15:04 PM.
This article is licensed under a Creative Commons Attribution-NonCommercial 3.0 Unported Licence.

interaction between the adsorbate and the surface of the adsorbent involving complexation reaction, surface adsorption, cation exchange, and electrostatic attraction.[27] Bandara *et al.* used biochar adsorbent, which was derived from agricultural wastes, to remove Cd(II) and Cu(II) ions from aqueous media. They found that the adsorption capacity of this adsorbent towards Cd(II) and Cu(II) ions is 6.28 and 18 mg g^{-1}, respectively.[28] Joseph *et al.* used FAU-type zeolite adsorbent, which was derived from coal fly ash, to remove Cd(II) and Cu(II) ions from aqueous media. They found that the adsorption capacity of this adsorbent towards Cd(II) and Cu(II) ions is 74.074 and 57.803 mg g^{-1}, respectively.[29] Ali *et al.* used thio-functionalized layered double hydroxide (Mn–MoS_4) adsorbent to remove Cd(II) and Cu(II) ions from aqueous media. They found that the adsorption capacity of this adsorbent towards Cd(II) and Cu(II) ions is 93.11 and 58.07 mg g^{-1}, respectively.[30] Hua *et al.* used Sulfhydryl functionalized hydrogel adsorbent to remove Cd(II) and Cu(II) ions from aqueous media. They found that the adsorption capacity of this adsorbent towards Cd(II) and Cu(II) ions is 27.40 and 15.60 mg g^{-1}, respectively.[31] Khalifa *et al.* developed a new adsorbent composed of silica nanoparticles enhanced with dibenzoylmethane to remove Cd(II) and Cu(II) ions from aqueous solutions. The adsorption capacity of this adsorbent for Cd(II) and Cu(II) ions was determined to be 35.37 and 31.76 mg g^{-1}, respectively.[32] Consequently, our research team aims to synthesizes new inorganic/organic nanocomposites *via* a simple procedure for efficient removal and preconcentration of Cd(II) and Cu(II) ions from water, blood, and fish muscles. The silica modified with (3-aminopropyl) triethoxysilane reacted with 2,4-dihydroxybenzaldehyde and 5-bromosalicylaldehyde to produce new inorganic/organic nanocomposites. In these nanocomposites, the inorganic support carries the organic molecules which form chelates with metal ions and thus facilitate their removal. The concentration of metal ions is often determined using atomic spectroscopic equipment such as flame atomic absorption spectrometry, graphite furnace atomic absorption spectrometry, and inductively coupled plasma optical emission spectrometry. Nevertheless, a preconcentration procedure is typically required before instrumental measurement in order to eliminate any predicted matrix influences and increase the instrument's sensitivity by reducing the detection limit. Several separating and preconcentration techniques, such as ionic liquid extraction, cloud point extraction, electrochemical deposition, ion exchange, coprecipitation, and solid phase extraction, are employed to achieve this objective. Owing to its simplicity, selectivity, and versatility, solid phase extraction is generally favored over alternative methods.[33] Before analyzing real samples with flame atomic absorption spectrometry, Cu(II) and Cd(II) ions were preconcentrated using the synthesized nanocomposites. Consequently, this research presents new and innovative environmental effects.

2. Experimental

2.1. Chemicals

Sodium metasilicate pentahydrate ($Na_2SiO_3 \cdot 5H_2O$), nitric acid (HNO_3), (3-aminopropyl)triethoxysilane ($C_9H_{23}NO_3Si$), ethanol (C_2H_6O), thiourea (CH_4N_2S), 2,4-dihydroxybenzaldehyde ($C_7H_6O_3$), 5-bromosalicylaldehyde ($C_7H_5BrO_2$), xylene (C_8H_{10}), hydrochloric acid (HCl), concentrated sulfuric acid (H_2SO_4), cadmium(II) chloride monohydrate ($CdCl_2 \cdot H_2O$), potassium chloride (KCl), sodium hydroxide (NaOH), copper(II) chloride dihydrate ($CuCl_2 \cdot 2H_2O$), and ethylenediaminetetraacetic acid disodium salt dihydrate ($C_{10}H_{14}N_2Na_2O_8 \cdot 2H_2O$) were obtained from Sigma Aldrich Company and consumed without additional refinement (purity = 99.99%).

2.2. Synthesis of 2,4-dihydroxybenzaldehyde/silica and 5-bromosalicylaldehyde/silica nanocomposites

Firstly, the SiO_2 nanoparticles were synthesized as the following; 80 g of sodium metasilicate pentahydrate was dissolved in 400 mL of distilled water. After that, pH was set at 9 then the formed gel was stirred for 1 h. Besides, the formed gel was separated and thoroughly washed several times with warm distilled water to get rid of sodium chloride. Moreover, the produced gel was dried at 60 °C for 12 h then ignited at 600 °C for 5 h to obtain SiO_2 nanoparticles. Secondly, SiO_2 sample was modified with (3-aminopropyl)triethoxysilane according to the method described by Khalifa *et al.*[32] as the following; 2 g of SiO_2 sample was refluxed at 150 °C with 2.20 mL of (3-aminopropyl) triethoxysilane in 60 mL of xylene for 24 h. Besides, the modified silica was separated and thoroughly washed repeatedly with warm ethanol and water then dried at 60 °C for 12 h. Lastly, 2 g of the SiO_2 sample, which was modified with (3-aminopropyl) triethoxysilane, was refluxed at 150 °C for 24 h with 30 mL ethanolic solution containing 2 g of 2,4-dihydroxybenzaldehyde or 5-bromosalicylaldehyde accompanied by a few droplets of sulfuric acid. Then, the formed nanocomposites were separated and thoroughly washed repeatedly with warm ethanol and water then dried at 60 °C for 12 h. The nanocomposites, which were synthesized using 2,4-dihydroxybenzaldehyde and 5-bromosalicylaldehyde, were abbreviated as N_1 and N_2, respectively.

2.3. Instrumentation

The X-ray diffraction (XRD) patterns of the SiO_2, 2,4-dihydroxybenzaldehyde/silica, and 5-bromosalicylaldehyde/silica samples were obtained utilizing an X-ray diffractometer (D8 Advance, Bruker, Billerica, Massachusetts, United States) equipped with K_α copper radiations with a wavelength of 0.15 nm. Also, the Fourier transform (FT-IR) spectra of the SiO_2, 2,4-dihydroxybenzaldehyde/silica, and 5-bromosalicylaldehyde/silica samples, were obtained utilizing Fourier transform infrared spectrophotometer (Nicolet, Waltham, Massachusetts, United States). The morphologies of the SiO_2, 2,4-dihydroxybenzaldehyde/silica, and 5-bromosalicylaldehyde/silica samples were examined utilizing scanning electron microscopy (SEM, JEOL, SEM-JSM-5410LV, Akishima, Tokyo, Japan). BET surface area, average pore radius, and total pore volume of the SiO_2, 2,4-dihydroxybenzaldehyde/silica, and 5-bromosalicylaldehyde/silica samples were determined utilizing a nitrogen gas sorption analyzer (Quantachrome, NOVA, Boynton Beach, United States). CHN analyses of the 2,4-dihydroxybenzaldehyde/silica and 5-bromosalicylaldehyde/

© 2022 The Author(s). Published by the Royal Society of Chemistry

Open Access Article. Published on 01 July 2022. Downloaded on 2/7/2026 3:15:04 PM.
This article is licensed under a Creative Commons Attribution-NonCommercial 3.0 Unported Licence.

silica nanocomposites were determined utilizing CHN Elemental Analyzer (PerkinElmer, 2400, Waltham, United States).

2.4. Removal of Cu(II) and Cd(II) ions from aqueous media

For studying the effect of pH, the pH values of 75 mL of 200 mg L^{-1} of Cu(II) or Cd(II) solutions were adapted to different values (from 4 to 6 in the case of Cu(II) ions or from 4 to7 in the case of Cd(II) ions) before the addition of nanocomposites using 0.1 M HCl or NaOH. After that, 0.15 g of the N_1 or N_2 nanocomposites is added to each Cu(II) or Cd(II) solution then the mixture was stirred for 180 min.

For studying the effect of time, the pH values of 75 mL of 200 mg L^{-1} of Cu(II) or Cd(II) solutions were adapted to 6 in the case of Cu(II) ions or 7 in the case of Cd(II) ions before the addition of nanocomposites. After that, 0.15 g of the N_1 or N_2 nanocomposites is added to each Cu(II) or Cd(II) solution then the mixture was stirred for different times (10–180 min).

For studying the effect of temperature, the pH values of 75 mL of 200 mg L^{-1} of Cu(II) or Cd(II) solutions were adapted to 6 in the case of Cu(II) ions or 7 in the case of Cd(II) ions before the addition of nanocomposites. After that, 0.15 g of the N_1 or N_2 nanocomposites is added to each Cu(II) or Cd(II) solution. The mixture was then stirred for 120 min at different temperatures (298–328 kelvins).

For studying the effect of concentration, the pH values of 75 mL of 50–200 mg L^{-1} of Cu(II) or Cd(II) solutions were adapted to 6 in the case of Cu(II) ions or 7 in the case of Cd(II) ions before the addition of nanocomposites. After that, 0.15 g of the N_1 or N_2 nanocomposites is added to each Cu(II) or Cd(II) solution. The mixture was then stirred for 120 min at 298 kelvins.

After completing the study of each of the previous effects, the N_1 or N_2 nanocomposites are separated using centrifugation. After that, the remaining concentrations of Cu(II) or Cd(II) ions in the filtrate are estimated using atomic absorption spectrophotometer.

The quantity of the adsorbed Cu(II) or Cd(II) ions per gram of the N_1 or N_2 nanocomposites (Q, mg g^{-1}) was calculated using eqn (1).

$$Q = [M_i - M_e] \times \frac{V}{W} \quad (1)$$

The % removal (% R) of the Cu(II) or Cd(II) ions using the N_1 or N_2 nanocomposites was calculated using eqn (2).

$$\%\ R = \frac{M_i - M_e}{M_i} \times 100 \quad (2)$$

where, M_i (mg L^{-1}) represents the initial concentration of Cu(II) or Cd(II) ions while M_e (mg L^{-1}) represents their equilibrium concentration in the filtrate. Besides, V (L) is the volume of Cu(II) or Cd(II) solution whereas W (g) is the quantity of the nanocomposites.

For studying the effect of desorption, 0.15 g of the N_1 or N_2 nanocomposites was stirred with 75 mL of 5 mg L^{-1} of Cu(II) or Cd(II) solution (pH = 6 in the case of Cu(II) ions or 7 in the case of Cd(II) ions) for 120 min. Besides, the N_1 or N_2 nanocomposites were separated using centrifugation then thoroughly washed repeatedly with distilled water to remove the non-adsorbed Cu(II) or Cd(II) ions. Also, the loaded nanocomposites with Cu(II) or Cd(II) ions were then stirred for 15 min with 5.00 mL of 0.50 M of different eluents (HCl, HNO_3, thiourea, and EDTA disodium salt). Moreover, for studying the reusability (three cycles of adsorption/desorption process), 0.15 g of the regenerated N_1 or N_2 nanocomposites was stirred for 120 min with 75 mL of 5 mg L^{-1} of Cu(II) or Cd(II) solution (pH = 6 in the case of Cu(II) ions or 7 in the case of Cd(II) ions). 0.5 M of EDTA disodium salt is used to regenerate the N_1 or N_2 nanocomposites after each cycle.

The % desorption (% D) using different eluents was calculated using eqn (3).

$$\%\ D = \frac{100 M_d V_d}{(M_i - M_e) V} \quad (3)$$

where, M_d (mg L^{-1}) is the concentration of Cu(II) or Cd(II) ions in the eluent whereas V_d (L) is the volume of the eluent.

The point of zero charge (pH_{PZC}) of the N_1 or N_2 nanocomposites was determined as revealed by Khalifa *et al.*[32] as the following; the pH values of 0.01 M of KCl solutions were adapted to different values ($pH_{initial}$ = 2–12) before the addition of the N_1 or N_2 nanocomposites using 0.1 M HCl or NaOH. After that, 0.15 g of the N_1 or N_2 nanocomposites was added to each KCl solution then the mixture was stirred for 6 h. After that, the N_1 or N_2 nanocomposites were separated using centrifugation. Then, the final pH values (pH_{final}) of the filtrates were determined. pH_{final} values were plotted against $pH_{initial}$ values. The pH_{pzc} is the pH_{final} level where a characteristic plateau was gotten.[32]

2.5. Preconcentration of real samples

Sea water (from Ras Elbar-Mediterranean Sea-Egypt) and tap water (from Benha City-Egypt) samples were collected and filtered using filter paper to remove any solid suspensions. After that, the samples were kept in containers made of polypropylene pre-washed with 10% nitric acid. The blood sample was placed in tubes containing K_2EDTA to prevent blood coagulation. The tilapia fish was purchased from a market in Benha City, Egypt. Then, the skin of the fish was removed, its muscles dried at 100 °C and it was stored in bags made of polyethylene. To accomplish a fast process, the previous real samples were digested utilizing a microwave-assisted acid digestion method. Using teflon digesting tubes, 0.6 g of dry sample was mixed with 2.5 mL of 30% hydrogen peroxide and 5 mL of nitric acid. After 10 min at room temperature, the tubes were sealed then heated according to the following one-step technique (power: 1650 W; temperature: 200 °C; ramp time: 12 min; cooling time: 12 min; hold time: 12 min). After cooling the tubes to room temperature, nearly all of the solutions were evaporated and then diluted to 75 mL with distilled water. In a conical flask, 75 mL of digested solution or water sample was

Open Access Article. Published on 01 July 2022. Downloaded on 2/7/2026 3:15:04 PM.
This article is licensed under a Creative Commons Attribution-NonCommercial 3.0 Unported Licence.

combined with 0.15 g of the N_1 or N_2 nanocomposite. The pH of the solution was adapted to 6 in the case of Cu(II) ions or 7 in the case of Cd(II) ions. Then, the contents were stirred for 120 min then the N_1 or N_2 nanocomposite was separated, dried, and transferred into a 25 mL beaker. After adding 5 mL of 0.5 M EDTA disodium salt, the mixture was stirred for 15 min to allow the studied metal ions to desorb. The filtrate was then analyzed for determining the concentration of studied metal ions using an atomic absorption spectrometer.

3. Results and discussion

3.1. Characterization of 2,4-dihydroxybenzaldehyde/silica and 5-bromosalicylaldehyde/silica nanocomposites

Fig. 1A–C represents the X-ray diffraction patterns of the SiO_2, N_1, and N_2 samples, respectively. The diffraction peaks showed that the formed silica nanoparticles and the average crystalline size (54.80 nm) were in good shape and size, which are confirmed by the JCPDS card number 00-039-1425 of cristobalite. Also, the results suggested that the silica nanoparticles had

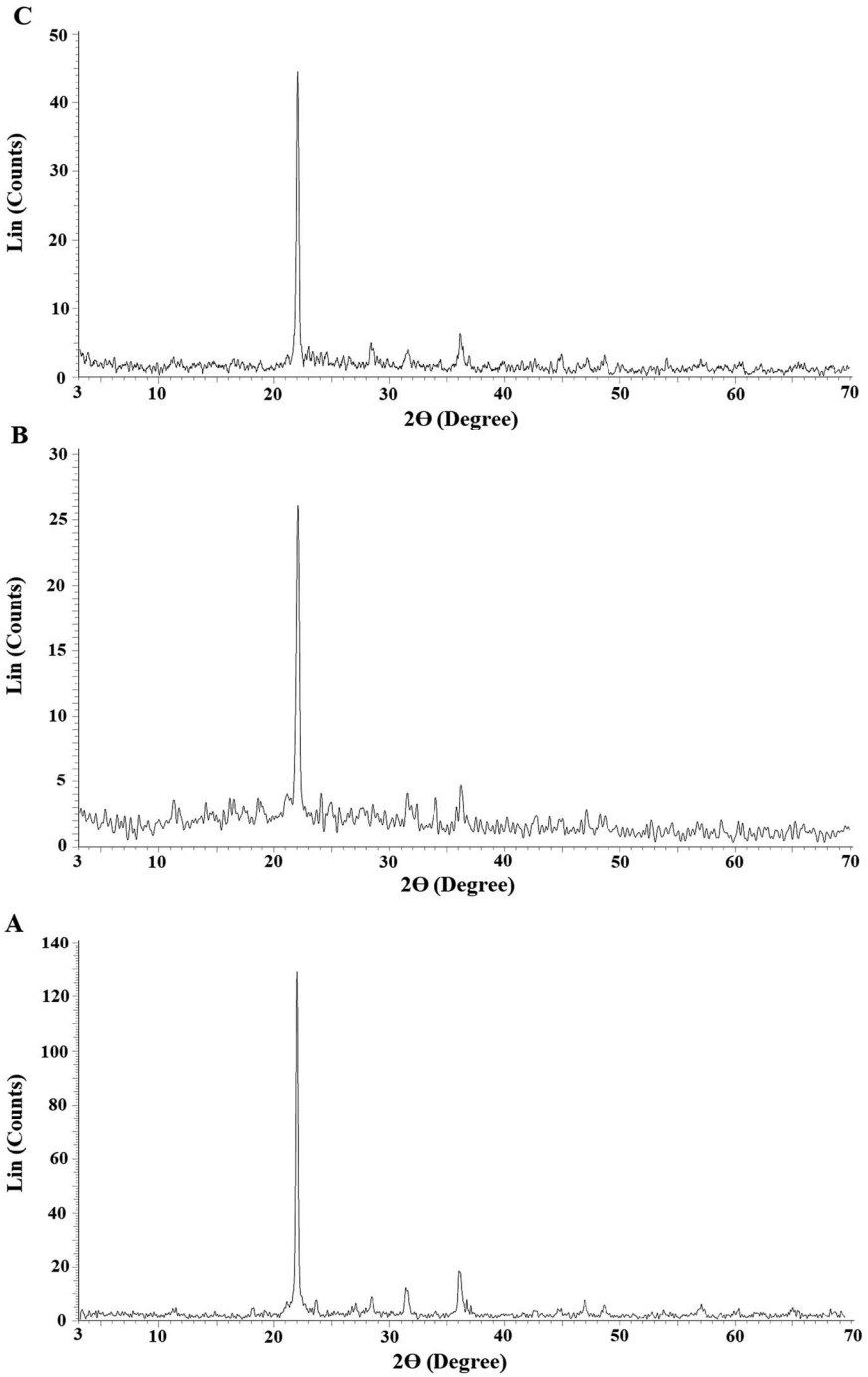

Fig. 1 The X-ray diffraction patterns of the SiO_2 (A), N_1 (B), and N_2 (C) samples.

© 2022 The Author(s). Published by the Royal Society of Chemistry

Open Access Article. Published on 01 July 2022. Downloaded on 2/7/2026 3:15:04 PM.
This article is licensed under a Creative Commons Attribution-NonCommercial 3.0 Unported Licence.

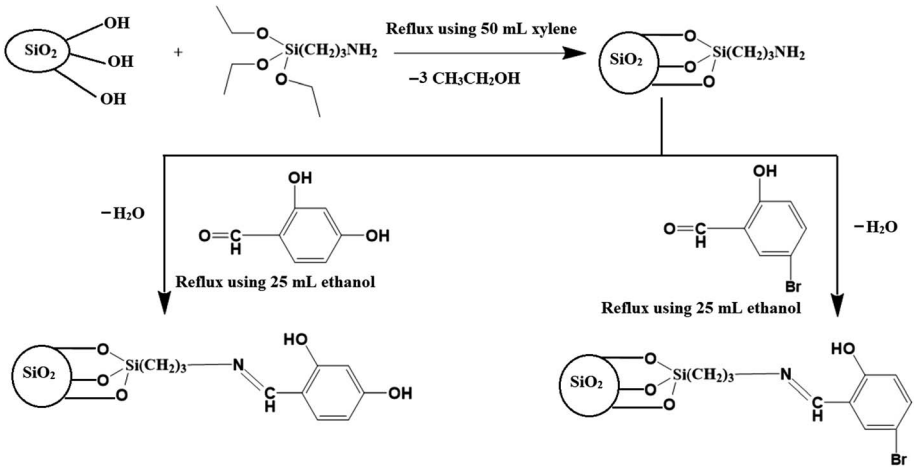

Scheme 1 The proposed structure of the synthesized nanocomposites.

a tetragonal structure.[34] Due to the formation of Schiff bases, as depicted in Scheme 1, the strength of the XRD peak at $2\theta = 21.9^{\circ}$ in the N_1 and N_2 nanocomposites decreased significantly. The FT-IR spectra of the SiO_2, N_1, and N_2 samples are depicted in Fig. 2A–C, respectively. The bands that appeared in the SiO_2, N_1, and N_2 samples at 468, 474, and 469 cm^{-1} are due to the bending vibration of O–Si–O, respectively. The bands that appeared in the SiO_2, N_1, and N_2 samples at 620 and 792 cm^{-1} are due to the symmetrical stretching vibration of Si–O–Si. The bands that appeared in the SiO_2, N_1, and N_2 samples at 1071, 1087, and 1073 cm^{-1} are due to the asymmetrical stretching vibration of Si–O–Si, respectively. The bands that appeared at 1620 and 3440 cm^{-1} in the SiO_2 sample are due to the bending and stretching vibration of OH, respectively.[35] The bands that appeared in the N_1 and N_2 samples at 1603 and 1629 cm^{-1}, are due to the bending vibration of C=N, respectively. The bands that appeared in the N_1 and N_2 samples at 3263 and 3260 cm^{-1} are due to the stretching vibration of OH, respectively. The bands that appeared in the N_1 and N_2 samples at 2940 and 2941 cm^{-1} are due to the stretching vibration of aliphatic CH, respectively. The bands that appeared in the N_1 and N_2 samples at 3003 and 3005 cm^{-1} are due to the stretching vibration of aromatic CH, respectively. The bands that appeared in the N_1 and N_2 samples in the range 1436–1506 cm^{-1} and 1435–1510 cm^{-1} are due to the stretching vibration of aromatic C=C, respectively. The band that appeared in the N_1 and N_2 samples at 1374 and 1377 cm^{-1} are due to the bending vibration of CH, respectively. The bands that appeared in the N_1 and N_2 samples in the range 845–920 and 918 cm^{-1} are due to the out-of-plane bending vibration of CH aromatic, respectively.[36] The slight displacement in the band positions of silica and the appearance of organic groups in the synthesized composites confirm the successful loading of the aforementioned organic materials on silica.

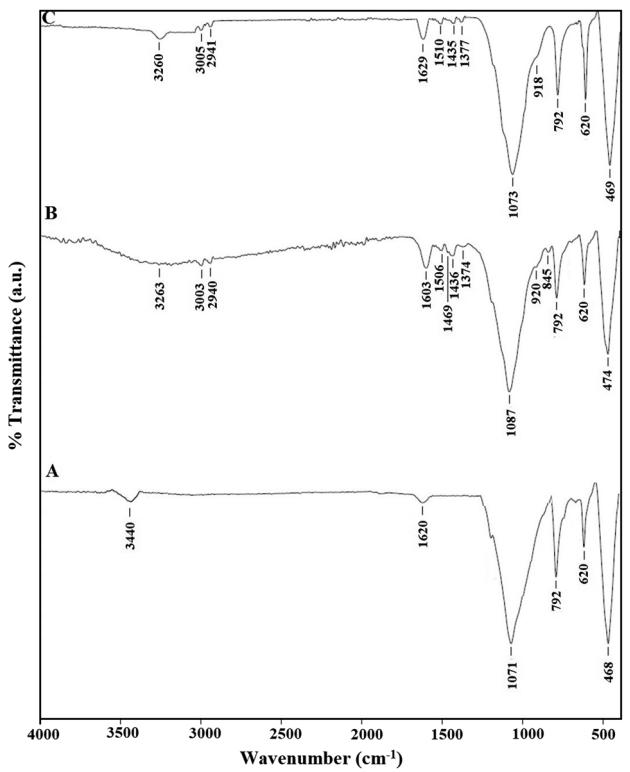

Fig. 2 The FT-IR spectra of the SiO_2 (A), N_1 (B), and N_2 (C) samples.

The percentages of carbon, hydrogen, and nitrogen in the N_1 nanocomposite were determined by elemental analysis to be 13.82, 3.50, and 1.53%, respectively. Also, the percentages of carbon, hydrogen, and nitrogen in the N_2 nanocomposite were determined by elemental analysis to be 12.67, 3.33, and 1.42%, respectively. Hence, the presence of carbon and nitrogen confirms the successful loading of the organic materials on the silica nanoparticles as revealed in Scheme 1. Also, Fig. 3A–D represents the N_2 adsorption/desorption isotherms of SiO_2, SiO_2/(3-aminopropyl)triethoxysilane, N_1, and N_2 samples, respectively. The results confirmed that the obtained isotherms belong to type IV.[37] Average pore size, BET surface area, and total pore volume were tabulated in Table 1. The total pore volume and BET surface area of the N_1 and N_2 nanocomposite were reduced because the formed Schiff base molecules block the pores of SiO_2. Consequently, this analysis confirms the

Open Access Article. Published on 01 July 2022. Downloaded on 2/7/2026 3:15:04 PM.
This article is licensed under a Creative Commons Attribution-NonCommercial 3.0 Unported Licence.

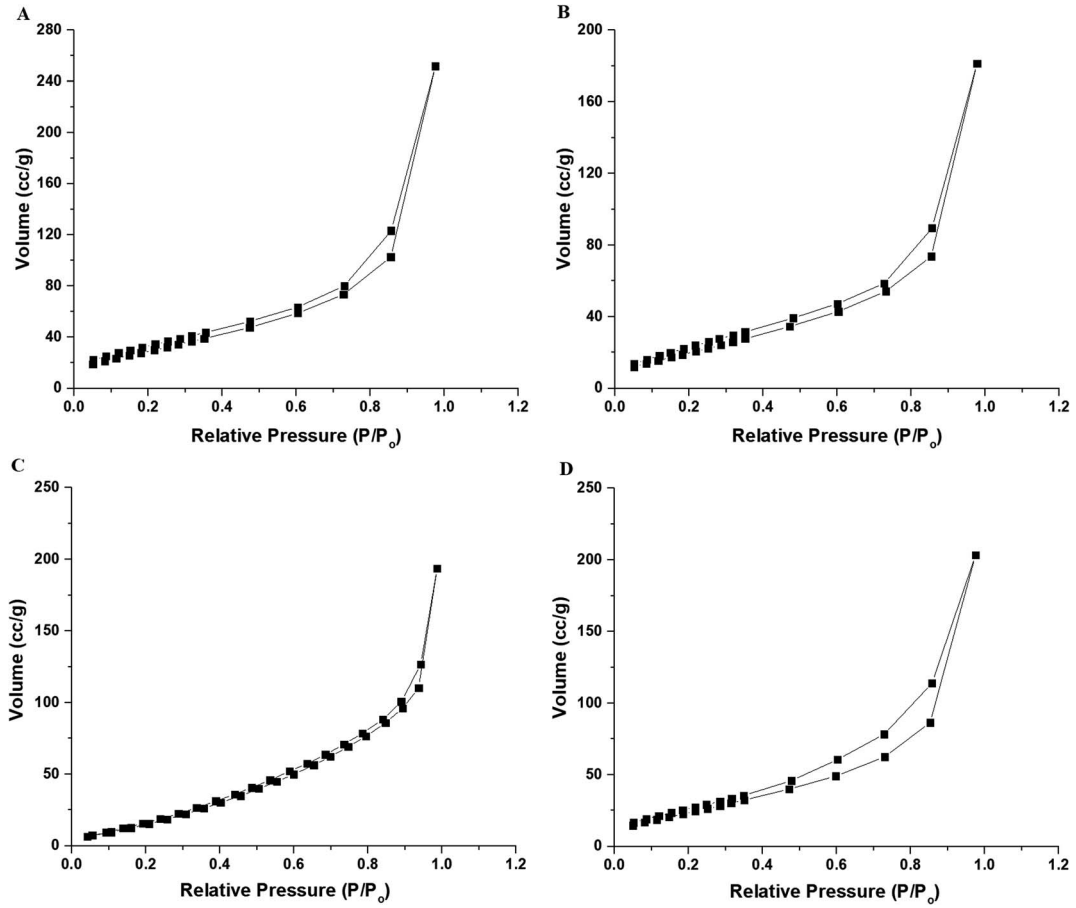

Fig. 3 The N_2 adsorption/desorption isotherms of the SiO_2 (A), SiO_2/(3-aminopropyl)triethoxysilane (B), N_1 (C), and N_2 (D) samples.

Table 1 Average pore size, BET surface area, and total pore volume of the synthesized samples

Sample	BET surface area ($m^2\ g^{-1}$)	Total pore volume ($cc\ g^{-1}$)	Average pore size (nm)
SiO_2	115.260	0.391	6.777
SiO_2/(3−aminopropyl) triethoxysilane	83.335	0.281	6.745
N_1	93.558	0.1491	3.188
N_2	96.282	0.315	6.553

successful loading of the Schiff bases on the silica nanoparticles as revealed in Scheme 1. Moreover, Fig. 4A–C represents the FE-SEM images of the SiO_2, N_1, and N_2 samples, respectively. Also, the FE-SEM analysis shows the morphology of the silica nanoparticles which identified as spherical and rod with slight agglomeration while the N_1 and N_2 nanocomposites have flaky surfaces due to the formation of C=N group.

3.2. Analytical factors that influence the removal of Cu(II) and Cd(II) ions from aqueous solutions

3.2.1. Effect of pH. Fig. 5A–B depicts the relationship between % *R* or *Q* ($mg\ g^{-1}$) and pH for Cu(II) and Cd(II) ions, respectively. In the case of Cu(II) ions, it was found that % *R* or *Q* using N_1 and N_2 nanocomposites increases with the increase in the pH value until it reached 59.60 and 39.20 at pH = 6, respectively. In the case of Cd(II) ions, it was found that % *R* or *Q* using N_1 and N_2 nanocomposites increases with the increase in the pH value until it reached 24.81 and 21.32 at pH = 7, respectively. Fig. 6A–B represents the plot of pH_{final} *versus* $pH_{initial}$ for several KCl solutions in the case of using N_1 and N_2 nanocomposites, respectively. Besides, the point of zero charge of the N_1 and N_2 nanocomposites is 3.27 and 3.20, respectively. If the pH of the Cu(II) or Cd(II) solution is less than point of zero charge of the nanocomposites, the surface of the nanocomposites are surrounded by positive hydrogen ions (H^+). Accordingly, % *R* decreases owing to repulsion between positive hydrogen ions and Cu(II) or Cd(II) ions. On the contrary, if the pH of the Cu(II) or Cd(II) solution is higher than point of the zero charge of the nanocomposites, the surface of the nanocomposites are surrounded by negative hydroxide ions (OH^-) which works to ionize the hydroxyl group of the composites easily and hence % *R* of Cu(II) or Cd(II) ions increases.[32]

3.2.2. Effect of time. Fig. 7A–B depicts the plot of % *R* or *Q* ($mg\ g^{-1}$) *versus* time in the case of Cu(II) and Cd(II) ions, respectively. In the case of Cu(II) ions, it was found that % *R* or *Q*

© 2022 The Author(s). Published by the Royal Society of Chemistry

Open Access Article. Published on 01 July 2022. Downloaded on 2/7/2026 3:15:04 PM.
This article is licensed under a Creative Commons Attribution-NonCommercial 3.0 Unported Licence.

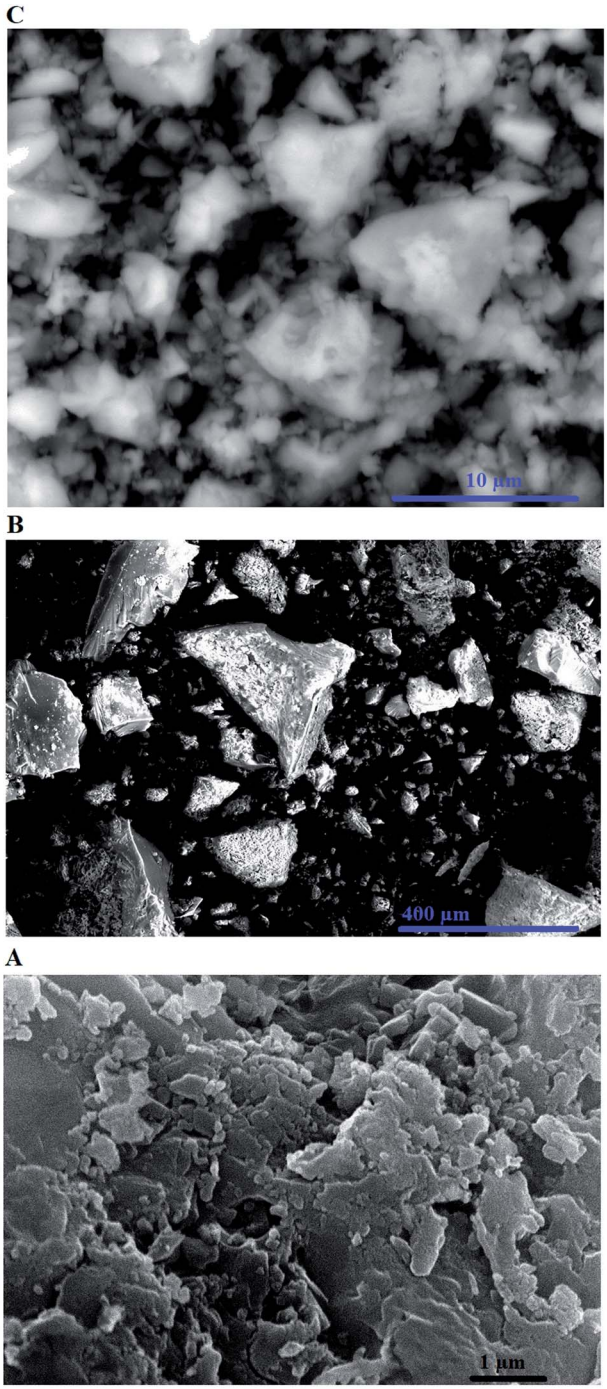

Fig. 4 The FE-SEM images of the SiO_2 (A), N_1 (B), and N_2 (C) samples.

using N_1 and N_2 nanocomposites increases with the increase in the time value until it reached 59.50 and 40.00 after 120 min, respectively. % R or Q was not affected when the time exceeded 120 min as a result of the saturation of the active sites. In the case of Cd(II) ions, it was found that % R or Q using N_1 and N_2 nanocomposites increases with the increase in the time value until it reached 25 and 22.50 after 120 min, respectively. Due to the saturation of the active sites when the time exceeded 120 min, neither % R nor Q was changed.

Our research group seeks to load organic materials that have not previously been loaded onto nanomaterials to study their effect on separation efficiency *via* the chelation method. In this regard, the effect of the presence of an electron-withdrawing groups such as Br in the para-position to OH by loading the 5-bromosalicylaldehyde material was studied. In addition, the effect of the presence of an electron-withdrawing group such as OH in the meta-position to OH by loading the 2,4-dihydroxybenzaldehyde material was studied. The presence of the bromine group in the para-position of OH makes the OH ionization relatively slow compared to the presence of the OH group in the meta-position of OH. The formation of chelates between loaded organic materials and studied metal ions is rapid in the case of the fast ionization of OH group and hence 2,4-dihydroxybenzaldehyde is superior to 5-bromosalicylaldehyde in removing the metal ions under study.

3.2.3. Effect of temperature. Fig. 8A–B depicts the plot of % R or Q (mg g^{-1}) *versus* temperature in the case of Cu(II) and Cd(II) ions, respectively. It was found that % R or Q using N_1 and N_2 nanocomposites decreases with the increase in the temperature. The optimal temperature, which will be considered for subsequent impacts, is therefore 298 K. The thermodynamic parameters, for example, change in free energy (ΔG^o), change in enthalpy (ΔH^o), and change in the entropy (ΔS^o) were determined using eqn (4) & (5).[21–26]

$$\ln K_T = \frac{\Delta S^o}{R} - \frac{\Delta H^o}{RT} \quad (4)$$

$$\Delta G^o = \Delta H^o - T\Delta S^o \quad (5)$$

where, T (K), K_T (L g^{-1}), and R (kJ mol^{-1} K^{-1}) are the temperature, distribution constant, and gas constant, respectively. The distribution constant (K_T) was determined utilizing eqn (6).[32]

$$K_T = \frac{Q_e}{M_e} \quad (6)$$

Fig. 9A–B depicts the relationship between $\ln K_T$ and T^{-1} for Cu(II) and Cd(II) ions, respectively. The correlation coefficients (R^2) in the case of using N_1 and N_2 samples for removing Cu(II) ions are 0.992 and 0.860, respectively. The correlation coefficients (R^2) in the case of using N_1 and N_2 samples for removing Cd(II) ions are 0.914 and 0.905, respectively. Hence, this confirms a strong relationship between $\ln K_T$ and $1/T$. The thermodynamic parameters are listed in Tables 2 and 3. The results clarified that the adsorption of Cu(II) or Cd(II) ions using the N_1 and N_2 nanocomposites is chemical because the value of ΔH^o is more than 40 kJ mol^{-1}.[32] Also, the adsorption of Cu(II) or Cd(II) ions using the N_1 and N_2 nanocomposites is exothermic owing to the negative sign of ΔH^o. The N_1 and N_2 nanocomposites can form chelates with Cu(II) or Cd(II) ions as clarified in Scheme 2. In addition, the spontaneous adsorption of Cu(II) or Cd(II) ions on N_1 and N_2 nanocomposites is due to the negative sign of ΔG^o. Moreover, the disordered adsorption of Cu(II) or Cd(II) ions at the solution boundary/nanocomposite is related to the positive sign of ΔS^o.

© 2022 The Author(s). Published by the Royal Society of Chemistry

Open Access Article. Published on 01 July 2022. Downloaded on 2/7/2026 3:15:04 PM.
This article is licensed under a Creative Commons Attribution-NonCommercial 3.0 Unported Licence.

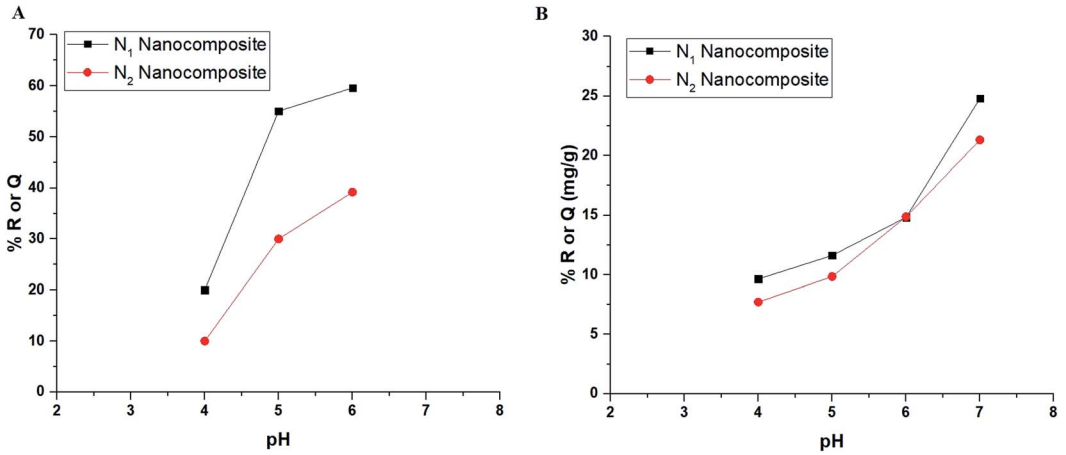

Fig. 5 The plot of % R or Q (mg g^{-1}) *versus* pH in the case of Cu(II) (A) and Cd(II) (B) ions.

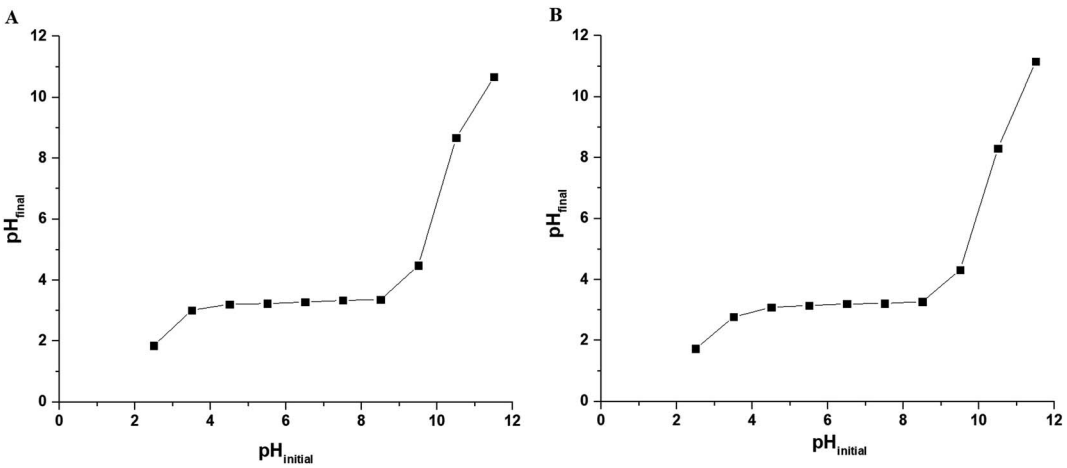

Fig. 6 The plot of pH_{final} *versus* $pH_{initial}$ for several KCl solutions in the case of using N_1 (A) and N_2 (B) nanocomposites.

3.2.4. Effect of concentration. Fig. 10A–B depicts the plot of the initial concentration of Cu(II) ions *versus* % *R* and *Q*, respectively. Besides, Fig. 11A–B depicts the plot of the initial concentration of Cd(II) ions *versus* % *R* and *Q*, respectively. It was found that % *R* decreases whereas *Q* increases with the increase in the initial concentration of Cu(II) or Cd(II) ions.[21–26]

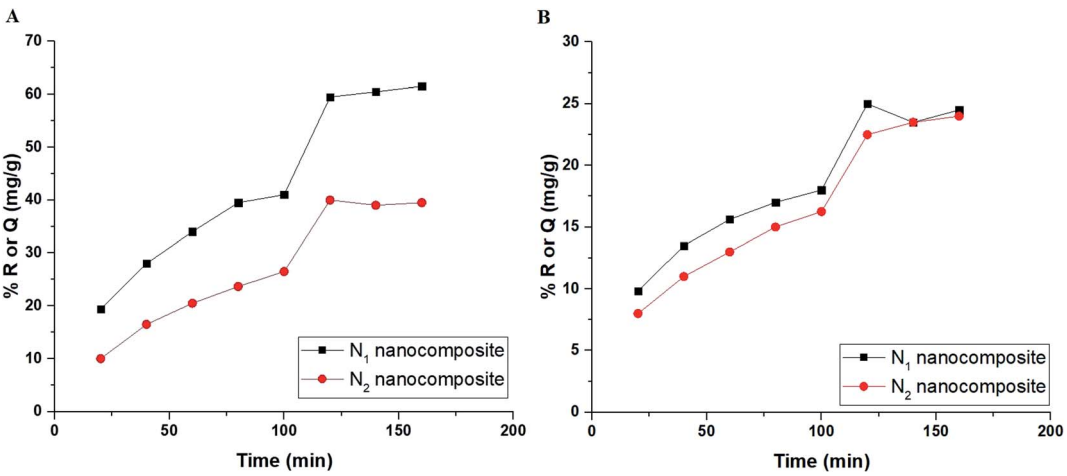

Fig. 7 The plot of % R or Q (mg g^{-1}) *versus* time in the case of Cu(II) (A) and Cd(II) (B) ions.

© 2022 The Author(s). Published by the Royal Society of Chemistry

Open Access Article. Published on 01 July 2022. Downloaded on 2/7/2026 3:15:04 PM.
This article is licensed under a Creative Commons Attribution-NonCommercial 3.0 Unported Licence.

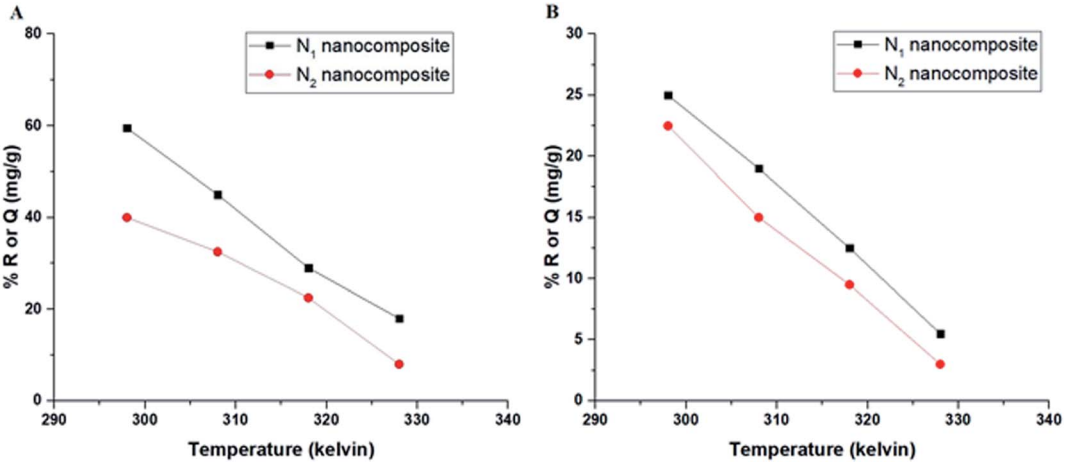

Fig. 8 The plot of % R or Q (mg g^{-1}) *versus* temperature in the case of Cu(II) (A) and Cd(II) (B) ions.

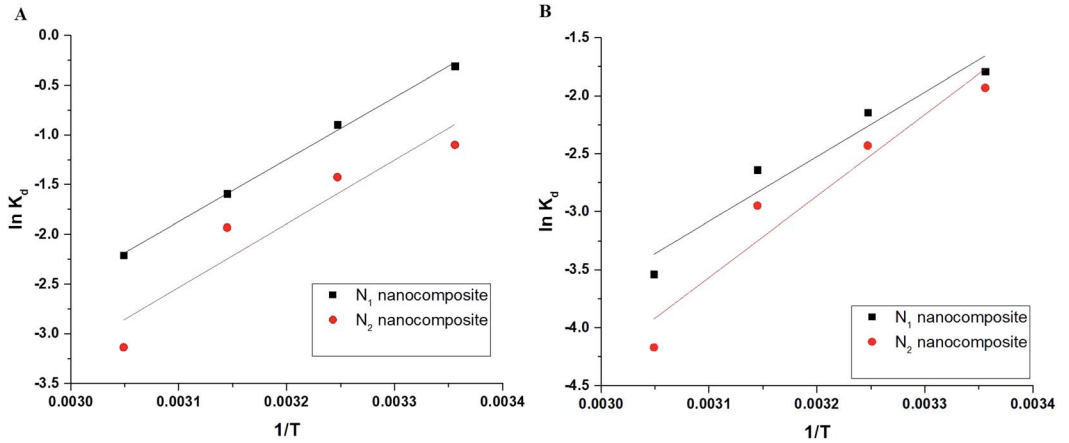

Fig. 9 The plot of $\ln K_T$ *versus* T^{-1} in the case of Cu(II) (A) and Cd(II) (B).

Table 2 Thermodynamic parameters in the case of Cu(II) ions

	ΔG^o (KJ mol^{-1})					
	Temperature (Kelvin)					
Sample	298	308	318	328	ΔS^o (KJ $mol^{-1}K^{-1}$)	ΔH^o (KJ mol^{-1})
N_1	−105.129	−106.905	−108.679	−110.455	0.178	−52.227
N_2	−109.376	−111.249	−113.121	−114.993	0.187	−53.576

Table 3 Thermodynamic parameters in the case of Cd(II) ions

	ΔGo (KJ mol^{-1})					
	Temperature (Kelvin)					
Sample	298	308	318	328	ΔSo (KJ $mol^{-1}K^{-1}$)	ΔHo (KJ mol^{-1})
N_1	−97.169	−98.869	−100.569	−102.268	0.169	−46.523
N_2	−121.862	−123.980	−126.099	−128.218	0.212	−58.729

The concentration-related results were studied by two equilibrium isotherms, namely: Langmuir (eqn (7)) and Freundlich (eqn (8)).[21–26]

$$\frac{M_e}{Q_e} = \frac{1}{P_4 Q_m} + \frac{M_e}{Q_m} \quad (7)$$

$$\ln Q_e = \ln P_5 + \frac{1}{L} \ln M_e \quad (8)$$

where, Q_m (mg g^{-1}) is the maximum adsorption capacity of the N_1 and N_2 nanocomposites. P_4 (L mg^{-1}) and P_5 (mg g^{-1}) (L

Open Access Article. Published on 01 July 2022. Downloaded on 2/7/2026 3:15:04 PM.
This article is licensed under a Creative Commons Attribution-NonCommercial 3.0 Unported Licence.

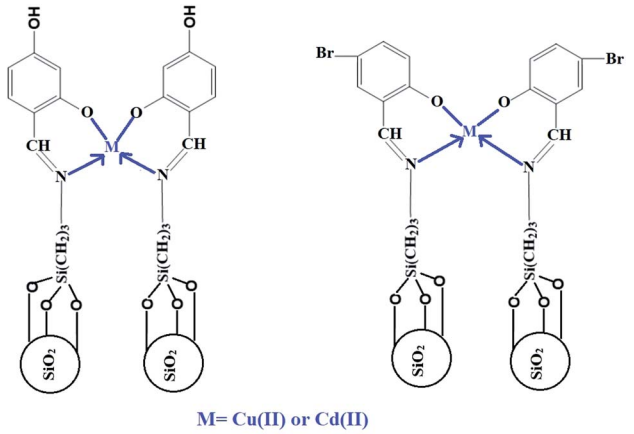

Scheme 2 The proposed mechanism for the adsorption of Cu(II) and Cd(II) ions.

$mg^{-1})^{1/L}$) refer to the Langmuir and Freundlich constants, respectively. L^{-1} refers to the heterogeneity constant. eqn (9) can be used to get the Q_m from the Freundlich isotherm.[21–26]

$$Q_m = P_5 (M_i^{1/L}) \quad (9)$$

Fig. 12A–B represents the Langmuir (the plot of M_e/Q_e *versus* M_e) and Freundlich (The plot of ln Q_e *versus* ln M_e) isotherms in the case of Cu(II) ions, respectively. Also, Fig. 13A–B represents the Langmuir (the plot of M_e/Q_e *versus* M_e) and Freundlich (the plot of ln Q_e *versus* ln M_e) isotherms in the case of Cd(II) ions, respectively. Also, the results confirmed that the correlation coefficients (R^2) of the Langmuir isotherm are larger than those of the Freundlich as shown in Tables 4 and 5. Therefore, the Langmuir isotherm better described equilibrium results than the Freundlich isotherm. The maximum adsorption capacity of the N_1 and N_2 nanocomposites toward Cu(II) ions is 64.81 and 40.93 mg g^{-1}, respectively. Also, the maximum adsorption capacity of the N_1 and N_2 nanocomposites toward Cd(II) ions is 27.39 and 26.34 mg g^{-1}, respectively. A comparison study was made between the adsorption capacity of the synthesized nanocomposites and that of other adsorbents such as biochar, FAU-type zeolite, thio-functionalized layered double hydroxide, sulfhydryl functionalized hydrogel, and silica/dibenzoylmethane

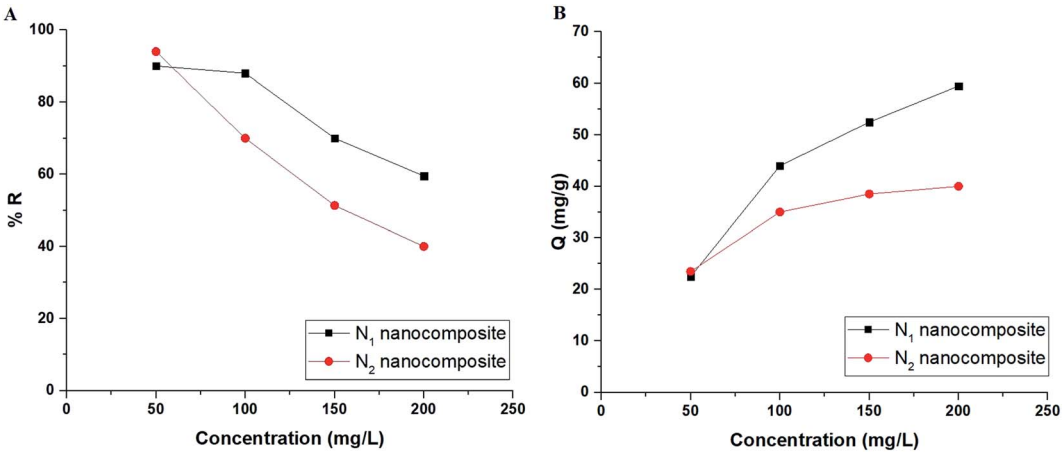

Fig. 10 The plot of initial concentration of Cu(II) ions *versus* % R (A) and Q (B).

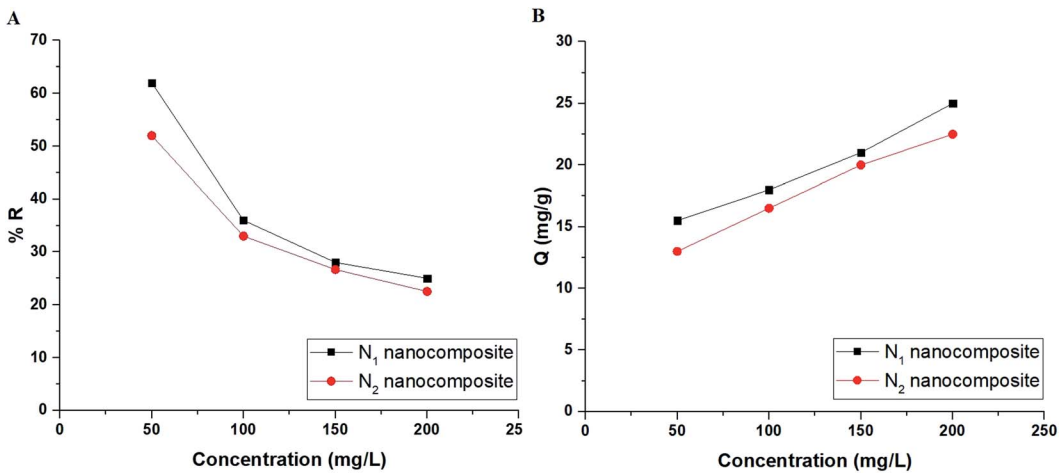

Fig. 11 The plot of initial concentration of Cd(II) ions *versus* % R (A) and Q (B).

© 2022 The Author(s). Published by the Royal Society of Chemistry

Open Access Article. Published on 01 July 2022. Downloaded on 2/7/2026 3:15:04 PM.
This article is licensed under a Creative Commons Attribution-NonCommercial 3.0 Unported Licence.

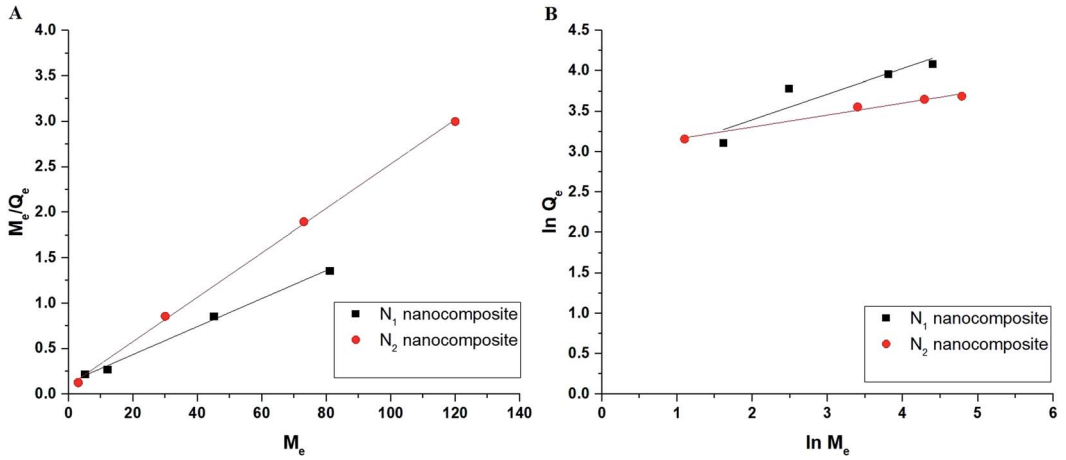

Fig. 12 The Langmuir (A) and Freundlich (B) isotherms in the case of Cu(II) ions.

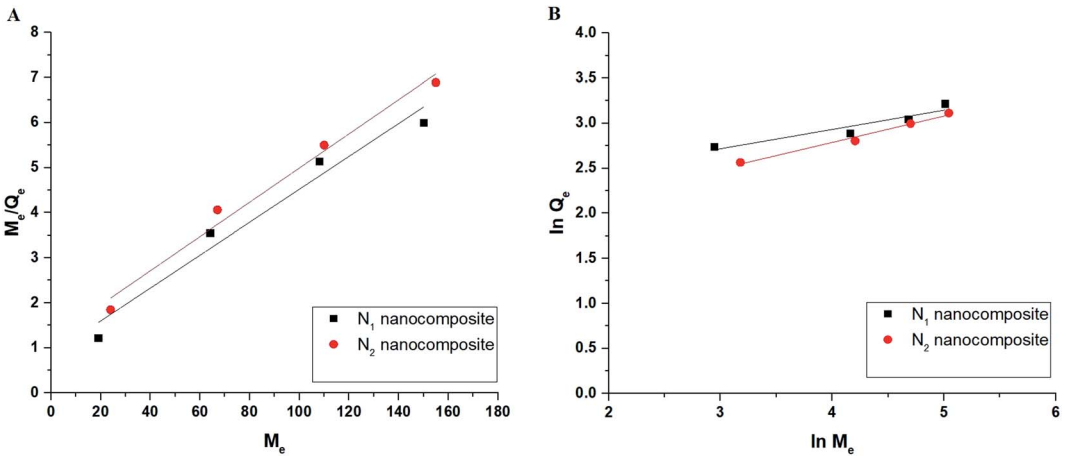

Fig. 13 The Langmuir (A) and Freundlich (B) isotherms in the case of Cd(II) ions.

Table 4 Equilibrium constants in the case of Cu(II) ions

	Langmuir			Freundlich		
Sample	Q_m (mg g^{-1})	P_4 (L mg^{-1})	R_2	Q_m (mg g^{-1})	P_5 (mg g^{-1})(L mg^{-1})1/L	R_2
N_1	64.81	0.122	0.994	84.78	15.85	0.7735
N_2	40.93	0.272	0.999	44.47	20.30	0.975

Table 5 Equilibrium constants in the case of Cd(II) ions

	Langmuir			Freundlich		
Sample	Q_m (mg g^{-1})	P_4 (L mg^{-1})	R_2	Q_m (mg g^{-1})	P_5 (mg g^{-1})(L mg^{-1})1/L	R_2
N_1	27.39	0.042	0.947	24.76	7.96	0.845
N_2	26.34	0.032	0.976	23.74	5.03	0.972

composite as shown in Table 6.[28–32,38–41] Clearly, the N_1 and N_2 nanocomposites outperformed the majority of adsorbents because they possess a high adsorption capacity.

3.2.5. Effect of desorption and reusability. Fig. 14A–B depicts the plot of % *D versus* some desorbing eluents in the case of Cu(II) and Cd(II) ions, respectively. The utilized

Open Access Article. Published on 01 July 2022. Downloaded on 2/7/2026 3:15:04 PM.
This article is licensed under a Creative Commons Attribution-NonCommercial 3.0 Unported Licence.

Table 6 A comparison study between the adsorption capacity of the synthesized nanocomposites and that of other adsorbents

Adsorbent	Adsorption capacity (mg g^{-1}) toward Cu(II) ions	Adsorption capacity (mg g^{-1}) toward Cd(II) ions	Ref.
Biochar	18	6.28	28
FAU-type zeolite	57.803	74.074	29
Thio-functionalized layered double hydroxide	58.07	93.11	30
Sulfhydryl functionalized hydrogel	15.60	27.40	31
Silica/dibenzoylmethane composite	31.76	35.37	32
Carbon gel/graphite composite	8.64	-	38
Arabica and robusta roasted coffee beans	2	2	39
Natural zeolite	2.5	1.5	40
natural clay	13.41	5.25	41
N_1 nanocomposite	64.81	27.39	This study
N_2 nanocomposite	40.93	26.34	This study

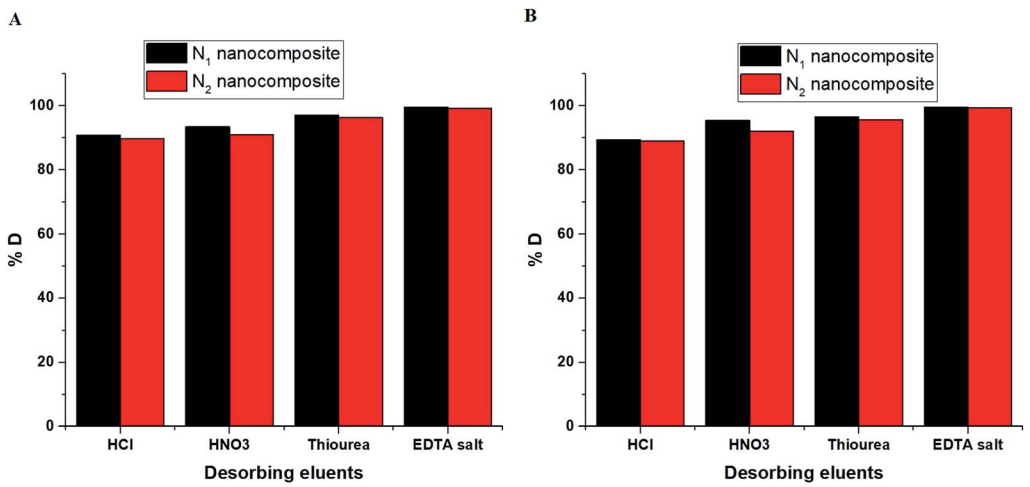

Fig. 14 The plot of % D *versus* some desorbing agents in the case of Cu(II) (A) and Cd(II) (B) ions.

desorbing eluents are 0.5 M of HCl, HNO_3, thiourea, and EDTA disodium salt. The results confirmed that 0.5 M of EDTA disodium salt is considered the appropriate desorbing eluent required for the maximum recovery (more than 99%) of the adsorbed Cu(II) or Cd(II) ions from the N_1 or N_2 nanocomposites. Fig. 15A–B depicts the plot of % *R versus* cycle

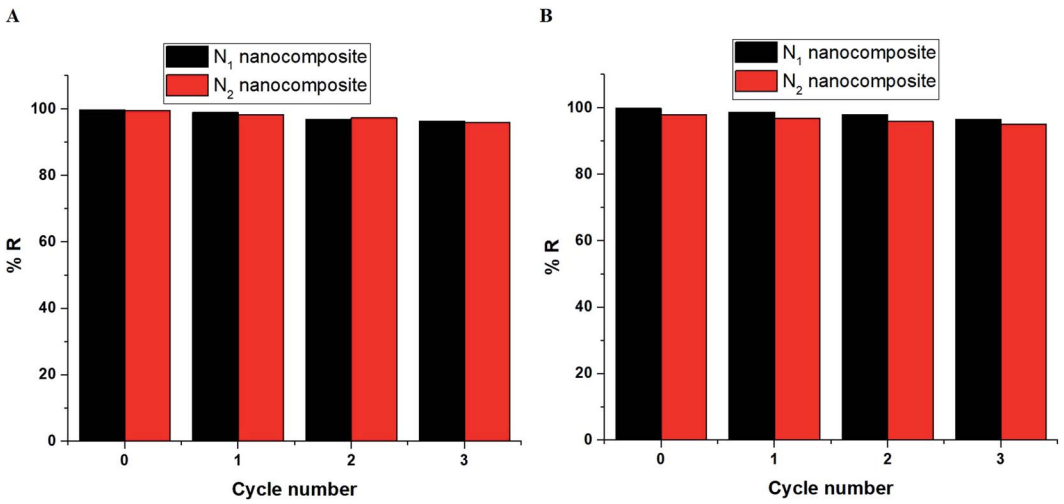

Fig. 15 The plot of % R or Q (mg g^{-1}) *versus* cycle number in the case of Cu(II) (A) and Cd(II) (B) ions.

© 2022 The Author(s). Published by the Royal Society of Chemistry

Open Access Article. Published on 01 July 2022. Downloaded on 2/7/2026 3:15:04 PM.
This article is licensed under a Creative Commons Attribution-NonCommercial 3.0 Unported Licence.

Table 7 Removal of Cu(II) and Cd(II) ions from binary mixtures using N_1 nanocomposite in the presence of different diverse ions

Diverse ion	Tolerance limit (mg L^{-1})	% R	
		Cu(II)	Cd(II)
K(I)	900	99.15	99.96
Na(I)	900	99.24	99.65
Ca(II)	120	98.38	99.08
Ba(II)	80	99.08	99.18
Mg(II)	120	97.17	99.00
Hg(II)	80	98.57	98.37
Fe(II)	120	97.39	99.14
Mn(II)	80	96.79	97.76
Ni(II)	80	95.87	96.79
Al(III)	80	98.16	98.45
Fe(III)	100	99.46	99.53
HCO^{3-}	1000	99.68	99.78
NO^{3-}	1000	99.73	99.65
Cl^-	1000	99.82	99.72
SO_4^{2-}	1000	99.18	99.64

Table 8 Removal of Cu(II) and Cd(II) ions from binary mixtures using N_2 nanocomposite in the presence of different diverse ions

Diverse ion	Tolerance limit (mg L^{-1})	% R	
		Cu(II)	Cd(II)
K(I)	900	99.26	99.78
Na(I)	900	99.37	99.89
Ca(II)	120	98.26	99.16
Ba(II)	80	99.65	99.32
Mg(II)	120	97.28	99.43
Hg(II)	80	98.54	98.52
Fe(II)	120	97.31	98.95
Mn(II)	80	96.64	98.15
Ni(II)	80	95.77	96.64
Al(III)	80	98.53	98.83
Fe(III)	100	99.36	99.73
HCO^{3-}	1000	99.47	99.58
NO^{3-}	1000	99.17	99.28
Cl^-	1000	99.63	99.71
SO_4^{2-}	1000	99.13	99.82

number in the case of Cu(II) and Cd(II) ions, respectively. The slight decrease in % R confirms that the synthesized N_1 and N_2 nanocomposites can be used successfully and several times in the removal of Cu(II) and Cd(II) ions from aqueous media.

3.2.6. Effect of co-existing ions. To determine the effect of various anions and cations on the extraction efficiency of Cu(II) and Cd(II) ions using the present method, the possible interfering ion was introduced at varying concentrations to a 75 mL solution containing 200 μg L^{-1} of each metal ion under investigation. The extraction technique was carried out using N_1 and N_2 nanocomposites precisely as described earlier, and its effectiveness was evaluated. The tolerance limit was established as the highest concentration of the accompanying ion that cause an error ≤5% in the recovery of Cu(II) or Cd(II) ions by the procedure. Tables 7 and 8 clearly illustrate that the majority of coexisting ions have a rather high tolerance limit, demonstrating the selectivity of the technique. Consequently, the method can be applied to the analysis of real samples including various components.

3.2.7. Application. Prior to atomic absorption spectrometer analysis, the proposed separation process was employed to preconcentrate Cu(II) and Cd(II) ions in real samples (sea water, tap water, fish muscles, and blood). The results of the preconcentration of Cu(II) using N_1 and N_2 nanocomposites, as well as the recoveries for the spiked samples, are presented in Tables 9 and 10, respectively. The results of the preconcentration of Cd(II) using N_1 and N_2 nanocomposites, as well as the recoveries for the spiked samples, are presented in Tables 11 and 12, respectively. % Recovery was calculated using eqn (10).

$$\%\ \text{Recovery} = \frac{\text{Found Concentration (Practically)}}{\text{Total Concentration (Theoretically)}} \times 100 \quad (10)$$

Also, % RSD (relative standard deviation) was calculated using eqn (11).

$$\%\ \text{RSD} = \frac{\text{Standard deviation}}{\text{Mean}} \times 100 \quad (11)$$

The recovery results indicate the process's precision, adaptability, and quantitative separation because the values of % recovery are more than 95%. In addition, the % RSD was less than 3.5%, showing excellent reproducibility.

Table 9 Determination of Cu(II) ions in real samples using N_1 nanocomposite

	Added volume from Cu(II) stock solution (1000 mg L^{-1})								
	0 mL			0.2 mL			0.4 mL		
Sample	Found concentration (mg L^{-1})	% Recovery	% RSD	Found concentration (mg L^{-1})	% Recovery	% RSD	Found concentration (mg L^{-1})	% Recovery	% RSD
Sea water	4.600 ± 0.124	—	2.174	7.040 ± 0.142	97.139	1.619	9.62 ± 0.309	97.362	2.589
Tap water	8.320 ± 0.492	—	2.150	10.816 ± 0.255	98.709	1.901	13.580 ± 0.492	99.993	2.918
Fish muscles	7.230 ± 0.247	—	2.749	9.820 ± 0.254	99.490	2.087	12.400 ± 0.351	99.226	2.281
Blood	1.090 ± 0.028	—	2.051	3.580 ± 0.104	95.551	2.337	6.358 ± 0.053	99.511	0.671

Open Access Article. Published on 01 July 2022. Downloaded on 2/7/2026 3:15:04 PM. This article is licensed under a Creative Commons Attribution-NonCommercial 3.0 Unported Licence.

Table 10 Determination of Cu(II) ions in real samples using N_2 nanocomposite

	Added volume from Cu(II) stock solution (1000 mg L^{-1})								
	0 mL			0.2 mL			0.4 mL		
Sample	Found concentration (mg L^{-1})	% Recovery	% RSD	Found concentration (mg L^{-1})	% Recovery	% RSD	Found concentration (mg L^{-1})	% Recovery	% RSD
Sea water	4.500 ± 0.124	—	2.222	6.990 ± 0.188	97.795	2.169	9.540 ± 0.272	97.534	2.297
Tap water	8.300 ± 0.152	—	1.476	10.876 ± 0.141	99.438	1.043	13.500 ± 0.412	99.550	2.457
Fish muscles	7.060 ± 0.225	—	2.573	9.660 ± 0.299	99.579	2.493	12.260 ± 0.208	99.451	1.365
Blood	1.082 ± 0.025	—	1.894	3.600 ± 0.088	96.290	1.964	6.280 ± 0.195	98.413	2.495

Table 11 Determination of Cd(II) ions in real samples using N_1 nanocomposite

	Added volume from Cd(II) stock solution (1000 mg L^{-1})								
	0 mL			0.2 mL			0.4 mL		
Sample	Found concentration (mg L^{-1})	% Recovery	% RSD	Found concentration (mg L^{-1})	% Recovery	% RSD	Found concentration (mg L^{-1})	% Recovery	% RSD
Sea water	0.184 ± 0.007	—	2.977	2.720 ± 0.104	95.671	3.076	5.390 ± 0.092	98.213	1.376
Tap water	0.146 ± 0.005	—	2.837	2.754 ± 0.063	98.168	1.844	5.372 ± 0.103	98.560	1.549
Fish muscles	21.100 ± 0.679	—	2.596	23.400 ± 0.519	98.719	1.788	26.200 ± 0.555	99.646	1.707
Blood	1.068 ± 0.037	—	2.762	3.564 ± 0.119	95.685	2.696	6.348 ± 0.132	99.696	1.672

Table 12 Determination of Cd(II) ions in real samples using N_2 nanocomposite

	Added volume from Cd(II) stock solution (1000 mg L^{-1})								
	0 mL			0.2 mL			0.4 mL		
Sample	Found concentration (mg L^{-1})	% Recovery	% RSD	Found concentration (mg L^{-1})	% Recovery	% RSD	Found concentration (mg L^{-1})	% Recovery	% RSD
Sea water	0.171 ± 0.006	—	2.905	2.740 ± 0.068	96.802	1.999	5.450 ± 0.088	99.534	1.297
Tap water	0.157 ± 0.006	—	2.848	2.774 ± 0.054	98.503	1.563	5.440 ± 0.142	99.612	2.096
Fish muscles	21.600 ± 0.473	—	1.763	24.000 ± 0.760	99.165	2.552	26.730 ± 0.890	99.774	2.683
Blood	1.078 ± 0.038	—	2.814	3.594 ± 0.089	96.232	2.002	6.334 ± 0.137	99.321	1.742

4. Conclusions

In this study, silica nanoparticles were modified by 2,4-dihydroxybenzaldehyde and 5-bromosalicylaldehyde to form N_1 and N_2 new nanocomposites, respectively. The nanocomposites were utilized for the removal and preconcentration of Cu(II) and Cd(II) ions from water, blood, and fish muscles. XRD, FT-IR, CHN elemental analyzer, FE-SEM, and nitrogen gas sorption analyzer were used to characterize the novel nanocomposites. The maximum adsorption capacity of the N_1 and N_2 nanocomposites toward Cu(II) ions is 64.81 and 40.93 mg g^{-1}, respectively. The maximum adsorption capacity of the N_1 and N_2 nanocomposites toward Cd(II) ions is 27.39 and 26.34 mg g^{-1}, respectively. The recovery findings demonstrate that the preconcentration process is accurate, adaptable, and resulted in quantitative separation (>95 percent). Furthermore, the % RSD was less than 3.5 percent, indicating good reproducibility.

Conflicts of interest

The authors confirm that there is no conflict of interest for this manuscript.

References

1 B. K. Mavakala, P. Sivalingam, A. Laffite, C. K. Mulaji, G. Giuliani, P. T. Mpiana and J. Poté, Evaluation of heavy metal content and potential ecological risks in soil samples from wild solid waste dumpsites in developing country under tropical conditions, *Environ. Challenges*, 2022, **7**, 100461.

2 M. A. Rahmat, A. F. Ismail, N. D. Rodzi, E. S. Aziman, W. M. R. Idris and T. Lihan, Assessment of natural radionuclides and heavy metals contamination to the environment: Case study of Malaysian unregulated tin-tailing processing industry, *Nucl. Eng. Technol.*, 2022, **54**(6), 2230–2243.

© 2022 The Author(s). Published by the Royal Society of Chemistry

Open Access Article. Published on 01 July 2022. Downloaded on 2/7/2026 3:15:04 PM.
This article is licensed under a Creative Commons Attribution-NonCommercial 3.0 Unported Licence.

3 M. A. Shamim, H. Zia, M. Zeeshan, M. Y. Khan and M. Shahid, Metal organic frameworks (MOFs) as a cutting-edge tool for the selective detection and rapid removal of heavy metal ions from water: Recent progress, *J. Environ. Chem. Eng.*, 2022, **10**, 106991.

4 M. M. Kwikima, S. Mateso and Y. Chebude, Potentials of agricultural wastes as the ultimate alternative adsorbent for cadmium removal from wastewater, *Sci. Afr.*, 2021, **13**, e00934.

5 M. Kumar, A. Kushwaha, L. Goswami, A. K. Singh and M. Sikandar, A review on advances and mechanism for the phycoremediation of cadmium contaminated wastewater, *Cleaner Engineering and Technology*, 2021, **5**, 100288.

6 T. Liu, Y. Lawluvy, Y. Shi, J. O. Ighalo, Y. He, Y. Zhang and P. Yap, Adsorption of cadmium and lead from aqueous solution using modified biochar: A review, *J. Environ. Chem. Eng.*, 2022, **10**, 106502.

7 K. Elewa, A. Belal, O. El Monayeri and A. F. Tawfic, Application of metal-organic framework (Zn-Ph-D CP) for copper ion removal from aqueous solution, *Ain Shams Eng. J.*, 2022, **13**, 101670.

8 B. Lv, Z. Zhao, X. Deng, C. Fang, B. Xing and B. Dong, Hydrodynamics and adsorption performance of liquid–solid fluidized bed with granular activated carbon for removal of copper ions from wastewater, *J. Cleaner Prod.*, 2021, **328**, 129627.

9 V. Krstić, T. Urošević and B. Pešovski, A review on adsorbents for treatment of water and wastewaters containing copper ions, *Chem. Eng. Sci.*, 2018, **192**, 273–287.

10 M. Zaynab, R. Al-Yahyai, A. Ameen, Y. Sharif, L. Ali, M. Fatima, K. A. Khan and S. Li, Health and environmental effects of heavy metals, *J. King Saud Univ., Sci.*, 2022, **34**, 101653.

11 S. Sandilyan and K. Kathiresan, Decline of mangroves - A threat of heavy metal poisoning in Asia, *Ocean Coast. Manag.*, 2014, **102**, 161–168.

12 J. Briffa, E. Sinagra and R. Blundell, Heavy metal pollution in the environment and their toxicological effects on humans, *Heliyon*, 2020, **6**, e04691.

13 Y. Zhang, L. Zhang, R. Gao, L. Zhong and J. Xue, $CaCO_3$-coated PVA/BC-based composite for the simultaneous adsorption of Cu(II), Cd(II), Pb(II) in aqueous solution, *Carbohydr. Polym.*, 2021, **267**, 118227.

14 Y. Ma, Z. Deng, Z. Li, Q. Lin, Y. Wu and W. Dou, Adsorption characteristics and mechanism for $K_2Ti_4O_9$ whiskers removal of Pb(II), Cd(II), and Cu(II) cations in wastewater, *J. Environ. Chem. Eng.*, 2021, **9**, 106236.

15 Q. Hou, H. Zhou, W. Zhang, Q. Chang, J. Yang, C. Xue and S. Hu, Boosting adsorption of heavy metal ions in wastewater through solar-driven interfacial evaporation of chemically-treated carbonized wood, *Sci. Total Environ.*, 2021, **759**, 144317.

16 K. Kalaitzidou, A. Zouboulis and M. Mitrakas, Cost evaluation for Se(IV) removal, by applying common drinking water treatment processes: Coagulation/precipitation or adsorption, *J. Environ. Chem. Eng.*, 2020, **8**, 104209.

17 L. Yang, W. Hu, Z. Chang, T. Liu, D. Fang, P. Shao, H. Shi and X. Luo, Electrochemical recovery and high value-added reutilization of heavy metal ions from wastewater: Recent advances and future trends, *Environ. Int.*, 2021, **152**, 106512.

18 A. M. Nasir, P. S. Goh, M. S. Abdullah, B. C. Ng and A. F. Ismail, Adsorptive nanocomposite membranes for heavy metal remediation: Recent progresses and challenges, *Chemosphere*, 2019, **232**, 96–112.

19 C. Zamora-Ledezma, D. Negrete-Bolagay, F. Figueroa, E. Zamora-Ledezma, M. Ni, F. Alexis and V. H. Guerrero, Heavy metal water pollution: A fresh look about hazards, novel and conventional remediation methods, *Environ. Technol. Innovation*, 2021, **22**, 101504.

20 E. A. Abdelrahman, D. A. Tolan and M. Y. Nassar, A Tunable Template-Assisted Hydrothermal Synthesis of Hydroxysodalite Zeolite Nanoparticles Using Various Aliphatic Organic Acids for the Removal of Zinc(II) Ions from Aqueous Media, *J. Inorg. Organomet. Polym. Mater.*, 2019, **29**, 229–247.

21 A. M. Hameed, A. Alharbi, E. A. Abdelrahman, E. M. Mabrouk, R. M. Hegazey, F. K. Algethami, Y. O. Al-Ghamdi and H. M. Youssef, Facile Hydrothermal Fabrication of Analcime and Zeolite X for Efficient Removal of Cd(II) Ions From Aqueous Media and Polluted Water, *J. Inorg. Organomet. Polym. Mater.*, 2020, **30**, 4117–4128.

22 E. A. Abdelrahman, A. Alharbi, A. Subaihi, A. M. Hameed, M. A. Almutairi, F. K. Algethami and H. M. Youssef, Facile fabrication of novel analcime/sodium aluminum silicate hydrate and zeolite Y/faujasite mesoporous nanocomposites for efficient removal of Cu(II) and Pb(II) ions from aqueous media, *J. Mater. Res. Technol.*, 2020, **9**, 7900–7914.

23 H. M. Youssef, R. K. Shah, F. K. Algethami, R. M. Hegazey, A. M. Naglah, M. A. Al-Omar, A. A. Alluhaybi, H. A. Alherbish, E. M. Mabrouk and E. A. Abdelrahman, Facile Hydrothermal Procedure for the Synthesis of Sodium Aluminum Silicate Hydrate/Analcime and Analcime for Effective Removal of Manganese(II) Ions From Aqueous Solutions, *J. Inorg. Organomet. Polym. Mater.*, 2021, **31**, 1035–1046.

24 E. A. Abdelrahman and R. M. Hegazey, Utilization of waste aluminum cans in the fabrication of hydroxysodalite nanoparticles and their chitosan biopolymer composites for the removal of Ni(II) and Pb(II) ions from aqueous solutions: Kinetic, equilibrium, and reusability studies, *Microchem. J.*, 2019, **145**, 18–25.

25 E. A. Abdelrahman, Y. G. Abou El-Reash, H. M. Youssef, Y. H. Kotp and R. M. Hegazey, Utilization of rice husk and waste aluminum cans for the synthesis of some nanosized zeolite, zeolite/zeolite, and geopolymer/zeolite products for the efficient removal of Co(II), Cu(II), and Zn(II) ions from aqueous media, *J. Hazard. Mater.*, 2021, **401**, 123813.

26 E. A. Abdelrahman and R. M. Hegazey, Exploitation of Egyptian insecticide cans in the fabrication of Si/Fe nanostructures and their chitosan polymer composites for

Open Access Article. Published on 01 July 2022. Downloaded on 2/7/2026 3:15:04 PM.
This article is licensed under a Creative Commons Attribution-NonCommercial 3.0 Unported Licence.

the removal of Ni(II), Cu(II), and Zn(II) ions from aqueous solutions, *Composites, Part B*, 2019, **166**, 382–400.

27 C. Duan, T. Ma, J. Wang and Y. Zhou, Removal of heavy metals from aqueous solution using carbon-based adsorbents: A review, *J. Water Process Eng.*, 2020, **37**, 101339.

28 T. Bandara, J. Xu, I. D. Potter, A. Franks, J. B. A. J. Chathurika and C. Tang, Mechanisms for the removal of Cd(II) and Cu(II) from aqueous solution and mine water by biochars derived from agricultural wastes, *Chemosphere*, 2020, **254**, 126745.

29 I. V. Joseph, L. Tosheva and A. M. Doyle, Simultaneous removal of Cd(II), Co(II), Cu(II), Pb(II), and Zn(II) ions from aqueous solutions *via* adsorption on FAU-type zeolites prepared from coal fly ash, *J. Environ. Chem. Eng.*, 2020, **8**, 103895.

30 J. Ali, H. Wang, J. Ifthikar, A. Khan, T. Wang, K. Zhan, A. Shahzad, Z. Chen and Z. Chen, Efficient, stable and selective adsorption of heavy metals by thio-functionalized layered double hydroxide in diverse types of water, *Chem. Eng. J.*, 2018, **332**, 387–397.

31 R. Hua and Z. Li, Sulfhydryl functionalized hydrogel with magnetism: Synthesis, characterization, and adsorption behavior study for heavy metal removal, *Chem. Eng. J.*, 2014, **249**, 189–200.

32 M. E. Khalifa, E. A. Abdelrahman, M. M. Hassanien and W. A. Ibrahim, Application of Mesoporous Silica Nanoparticles Modified with Dibenzoylmethane as a Novel Composite for Efficient Removal of Cd(II), Hg(II), and Cu(II) Ions from Aqueous Media, *J. Inorg. Organomet. Polym. Mater.*, 2020, **30**, 2182–2196.

33 I. M. M. Kenawy, Y. G. Abou El-Reash, M. M. Hassanien, N. R. Alnagar and W. I. Mortada, Use of microwave irradiation for modification of mesoporous silica nanoparticles by thioglycolic acid for removal of cadmium and mercury, *Microporous Mesoporous Mater.*, 2018, **258**, 217–227.

34 S. Xue, H. Xie, H. Ping, Q. Li, B. Su and Z. Fu, Induced Transformation of Amorphous Silica to Cristobalite on Bacterial Surface, *RSC Adv.*, 2015, **5**, 71844–71848.

35 V. Correcher, J. Garcia-Guinea, M. A. Bustillo and R. Garcia, Study of the thermoluminescence emission of a natural α-cristobalite, *Radiat. Eff. Defects Solids*, 2009, **164**, 59–67.

36 Z. P. Xu and P. S. Braterman, High affinity of dodecylbenzene sulfonate for layered double hydroxide and resulting morphological changes, *J. Mater. Chem.*, 2003, **13**, 268–273.

37 E. A. Abdelrahman, R. M. Hegazey and R. E. El-Azabawy, Efficient removal of methylene blue dye from aqueous media using Fe/Si, Cr/Si, Ni/Si, and Zn/Si amorphous novel adsorbents, *J. Mater. Res. Technol.*, 2019, **8**(6), 5301–5313.

38 M. Osińska, Removal of lead(II), copper(II), cobalt(II) and nickel(II) ions from aqueous solutions using carbon gels, *J. Sol-Gel Sci. Technol.*, 2017, **81**, 678–692.

39 E. Lichtfouse, J. Schwarzbauer and D. Robert, *Environmental chemistry*, Springer, 2001, pp. 119–259, DOI: **10.1021/ed078p1169**.

40 N. Elboughdiri, The use of natural zeolite to remove heavy metals Cu(II), Pb(II) and Cd(II), from industrial wastewater, *journal Cogent Engineering*, 2020, **7**, 1782623.

41 B. Abbou, I. Lebkiri, H. Ouaddari, L. Kadiri, A. Ouass, A. Habsaoui, A. Lebkiri and E. H. Rifi, Removal of Cd(II), Cu(II), and Pb(II) by adsorption onto natural clay: A kinetic and thermodynamic study, *Turk. J. Chem.*, 2021, **45**, 362–376.

© 2022 The Author(s). Published by the Royal Society of Chemistry